NAK associated protein 1 is required to activate Tank binding kinase 1 to regulate mitosis

Swagatika Paul[1], Shireen A. Sarraf[2], Leila Zavar[3], Lauren E. Fritsch[4], Nicole DeFoor[3], Alban Ordureau[5], and Alicia M. Pickrell[3, #]

[1]Graduate Program in Biomedical and Veterinary Sciences, Virginia-Maryland College of Veterinary Medicine, Blacksburg, VA 24061 USA [2]Biochemistry Section, National Institutes of Neurological Disorders and Stroke, National Institutes of Health, Bethesda, MD 20892 USA [3]School of Neuroscience, Virginia Polytechnic Institute and State University, Blacksburg, VA 24061 USA [4]Translational Biology, Medicine, and Health Graduate Program, Virginia Tech, Roanoke, VA 24016 USA [5]Cell Biology Program, Sloan Kettering Institute, New York, NY 10065 USA

Correspondence should be addressed to:

Alicia M. Pickrell, Life Science I Room 217, 970 Washington Street SW, Blacksburg, VA 24061

Tel: 540-232-8465; Email: alicia.pickrell@vt.edu

Keywords: NAP1, AZI2, TBK1, mitosis, cytokinesis

Running Title: NAP1 activates TBK1 during mitosis.

Abstract:

Mitosis is a precisely regulated cellular mechanism that governs fundamental processes like embryogenesis, development, and tissue regeneration. Prenatal mitotic errors can cause birth defects, including neurodevelopmental disorders, congenital heart disease, and miscarriage, whereas postnatal abnormal cell division leads to early tissue aging and tumorigenesis. Aberrant expression of the serine/threonine kinase, TANK-Binding Kinase 1 (TBK1), is associated with several types of cancers, such as glioblastomas, breast, and lung cancers. However, its role in normal cell division is not well understood. To better define mechanistically how TBK1 is activated during mitosis, we identified NAK-associated protein 1 (NAP1/AZI2) to be essential for mitosis. Loss of NAP1 reduces mitosis and cell proliferation resulting in the accumulation of multinucleated cells phenocopying the loss of TBK1. NAP1 is further responsible for the activation of TBK1 at centrosomes of dividing cells and required for proper mitotic progression. Furthermore, NAP1 expression during mitosis is mediated by the ubiquitin proteasome system. We have uncovered a distinct function for the NAP1-TBK1 complex during mitosis, completely novel from its previously known function in innate immunity.

Introduction:

TBK1 selectively translocates to and is activated at different organelles regulating diverse cell signaling programs, including the innate immune response (Fitzgerald et al., 2003; Pomerantz and Baltimore, 1999; Tojima et al., 2000), mitophagy (selective autophagic degradation of mitochondria) (Heo et al., 2015; Lazarou et al., 2015; Moore and Holzbaur, 2016; Richter et al., 2016; Vargas et al., 2019; Wong and Holzbaur, 2014), xenophagy (selective autophagic degradation of pathogens) (Ravenhill et al., 2019; Thurston et al., 2009; Wild et al.,

2011), and mitosis (Kim et al., 2013; Onorati et al., 2016; Pillai et al., 2015; Sarraf et al., 2019). TBK1 is necessary for proper progression through mitosis where it is activated at the centrosomes of dividing cells (Pillai *et al.*, 2015; Sarraf *et al.*, 2019) . The loss of TBK1 impairs mitosis leading to aberrant cell division and the accumulation of multinucleated cells (Maan et al., 2021; Pillai *et al.*, 2015; Sarraf *et al.*, 2019).

Activated TBK1 is sequestered to different organelles or regions of the cell in a seemingly exclusive manner. For example, during mitophagy, in which active TBK1 is localized to mitochondria, mitosis is impeded due to the unavailability of TBK1 to act at the centrosomes (Sarraf *et al.*, 2019). Similarly, infection by Zika virus sequesters activated TBK1 away from the centrosomes and directs it to mitochondria and the Zika particles which disrupts mitosis in neural epithelial stem cells and radial glia (Onorati *et al.*, 2016). This suggests that recruitment and activation of TBK1 at the centrosomes is crucial for successful completion of mitosis.

The crystal structure of TBK1 indicates that an adaptor protein is required for its activation (Fu et al., 2018; Larabi et al., 2013; Li et al., 2016; Zhang et al., 2019). Binding of an adaptor protein induces a conformational change of TBK1, resulting in its autophosphorylation at serine 172 and activation of the kinase domain after dimerization (Fu et al., 2021; Larabi *et al.*, 2013; Li *et al.*, 2016). This binding of the adaptor protein also drives TBK1's subcellular localization to different organelles to regulate these distinct signaling pathways (Goncalves et al., 2011; Heo *et al.*, 2015; Thurston et al., 2016). TBK1 has multiple binding partners/adaptors in immune signaling crucial for its activation, for example TANK, SINTBAD, NAP1/AZI2, Optineurin (OPTN), and STING (Bakshi et al., 2017; Clark et al., 2011; Fujita et al., 2003; Gatot et al., 2007; Gleason et al., 2011; Goncalves *et al.*, 2011; Ryzhakov and Randow, 2007; Tanaka and Chen, 2012; Zhang *et al.*, 2019). The TBK1-adaptor complexes then further phosphorylate

downstream targets such as IRF-3 and IRF-7 transcription factors (Fitzgerald *et al.*, 2003; Hemmi et al., 2004; Iwamura et al., 2001; Liu et al., 2015) thus inducing an immune response. OPTN, TAX1BP1, and NDP52, activate and recruit TBK1 to damaged mitochondria driving mitophagy (Heo *et al.*, 2015; Lazarou *et al.*, 2015; Moore and Holzbaur, 2016; Richter *et al.*, 2016). However, the adaptor or adaptors required for TBK1 activation and recruitment during mitosis are unknown.

We discovered the TBK1 adaptor protein, NAP1/AZI2, to be required during mitosis, whose function has only been described in innate immunity to trigger Type I interferon or NF-κB signaling. NAP1 is required for proper cell division by regulating TBK1 activation at the centrosomes during mitosis. Loss of NAP1 and TBK1 result in the accumulation of multinucleated cells, and induces mitotic and cytokinetic defects. Like many cell cycle regulatory proteins, expression of NAP1/AZI2 is tightly regulated during mitosis by the ubiquitin proteasome system (UPS). This NAP1-TBK1 signaling axis during mitosis is unique to its function in innate immunity.

Results

NAP1/AZI2 is required for TBK1 activation during mitosis.

Activation of TBK1 is reliant upon binding to adaptor proteins, which initiates higher order oligomerization of the TBK1-adaptor complex leading to trans-autophosphorylation at serine 172 (p-TBK1) (Fu *et al.*, 2018; Larabi *et al.*, 2013; Ma et al., 2012). The adaptor or adaptors required for TBK1 during miosis are unknown. Therefore, we screened known TBK1 adaptors to determine whether any of these proteins were responsible for its activation during mitosis. We investigated the TBK1 adaptors required in innate immune signaling by generating cell lines in which these proteins were stably knocked down (KD) using lentiviral-delivered

shRNA in HeLa cells (**Figure 1A-C**). Deficiency of TANK and SINTBAD did not alter the level of activated TBK1 (p-TBK1) during mitosis (**Figure 1D-E**); however, NAP1 KD did result in a reduction of p-TBK1 during mitosis (**Figure 1F**). We also assessed p-TBK1 levels in an NDP52/OPTN double KO (DKO) HeLa cell line as both adaptor proteins have been implicated in TBK1 activation during mitophagy and xenophagy (Heo *et al.*, 2015; Lazarou *et al.*, 2015; Moore and Holzbaur, 2016; Pourcelot et al., 2016; Ravenhill *et al.*, 2019; Richter *et al.*, 2016; Thurston *et al.*, 2009; Vargas *et al.*, 2019; Wild *et al.*, 2011; Wong and Holzbaur, 2014) and again found no difference between p-TBK1 levels during mitosis (**Figure S1A**). This was also true for a cell line lacking five autophagy related adaptors: NBR1, TAX1BP1, OPTN, p62, and NDP52 (**Figure S1B**). In conclusion, deficiency of NAP1 led to reduced activation of TBK1 in mitotic cells suggesting that NAP1 is the required adaptor for TBK1 activity.

NAP1 KO cells have mitotic and cytokinetic defects similar to TBK1 KO cells.

To confirm that TBK1 activation during mitosis was dependent on the loss of NAP1, we generated two independent NAP1 CRISPR knockout (KO) HeLa cell lines with multiple deletions in exon 4**.** We also attempted to use the non-transformed RPE-1 cell line to perform these studies, but were unable to generate either a CRISPR-mediated NAP1 KO or a stable shRNA-mediated NAP1 KD due to excessive cell death in the near-diploid cell line (**data not shown**). Both NAP1 KO clones displayed a decrease in p-TBK1 S172 (hereafter referred to as p-TBK1) levels on western blots during mitosis (**Figure 2A**). The intensity of p-TBK1 staining on the centrosomes was also significantly reduced in NAP1 KO cells as compared to HeLa (**Figure 2B-C**).

Previously, we and others have shown that loss of TBK1 led to growth defects, decreased number of mitotic cells, and an increased prevalence of multinucleated cells (Kim *et al.*, 2013;

Onorati *et al.*, 2016; Pillai *et al.*, 2015; Sarraf *et al.*, 2019). Therefore, we investigated the cell division pattern of NAP1 KO cells for comparison. Loss of NAP1 produced phenotypes similar to the loss of TBK1. In asynchronous conditions, NAP1 KO cells exhibited slower growth rates, fewer number of mitotic cells, an increase in the number of multinucleated cells, and cells undergoing mitosis (**Figure 2D-G**). We further characterized these mitotic defects between TBK1 and NAP1 KO cells seeing a significant prevalence of monopolar spindles and splayed/unfocused spindle poles in both genotypes, while TBK1 KO had significantly higher percentage of acentric fragments and NAP1 KO cells had a higher percentage of cells with more multipolar spindles (**Figure 2H-I**). Upon re-expression of NAP1, p-TBK1 levels were restored during mitosis in the NAP1 KO cells (**Figure 2J**).

There was a significantly higher percentage of cytokinetic cells in both TBK1 and NAP1 KO lines (**Figure S2A**). Upon detailed examination, we observed that these genotypes also had a higher percentage of cells with cytokinetic defects (**Figure S2B**). To further characterize how NAP1 and TBK1 regulate progression of cell division, we evaluated the types of cytokinetic defects in TBK1 and NAP1 KO cells. Both the KO cell lines exhibited unequal cytokinesis, as well as multipolar cytokinesis at a higher percentage than the parental line (**Figure S2 C-D**).

RNA-seq and northern blotting data have demonstrated that NAP1 is expressed ubiquitously in multiple different tissue types (Fagerberg et al., 2014; Fujita *et al.*, 2003). NAP1 was expressed in all human tissues probed on the protein level except for small intestine, in which there was little detectable NAP1 protein (**Figure S3A**) corroborating the previously reported mRNA levels in tissue (Fujita *et al.*, 2003). IKK-ß is a kinase reported to be involved in TBK1 activation (Clark et al., 2009); however, pharmacological inhibition of IKK-ß did not impact the levels of p-TBK1 present during mitosis (**Figure S3B**). NAP1 levels were also

unaffected in TBK1 KO cells (**Figure S3C**). These results suggest that NAP1 is a ubiquitously expressed protein that regulates mitosis and cytokinesis upstream of TBK1.

Phosphorylated TBK1 selectively interacts with NAP1 during mitosis.

To verify the interaction between NAP1 and TBK1 during mitosis, immunoprecipitation experiments were performed with either full length GFP-NAP1 (N' EGFP FL NAP1) or GFP-NAP1 lacking the TBK1 binding domain (N' EGFP NAP1 Δ200-270) (Ryzhakov and Randow, 2007) (**Figure 3A**). Endogenous phosphorylated TBK1 was enriched upon immunoprecipitation of N' EGFP FL NAP1 with substantially increased binding during mitosis when transiently overexpressed in HEK293T cells (**Figure 3B**). However, binding of activated TBK1 was abolished when the TBK1 binding domain of NAP1 (NAP1 Δ200-270) (Ryzhakov and Randow, 2007) was deleted in both asynchronous and mitotic conditions (**Figure 3B-C**). We next stably expressed two different N'FLAG-HA-TBK1 rescue constructs (**Figure 3A**) in TBK1 HeLa KO cells as our previous data indicated that TBK1 levels are tightly regulated inside the cell (see discussion)(Sarraf *et al.*, 2019). Endogenous NAP1 was enriched upon immunoprecipitation of full length TBK1 during mitosis compared to asynchronous conditions when normalized to the amount of TBK1 immunoprecipitated (**Figure 3D-E**). This binding did not occur in rescue lines when the known C-terminal TBK1 adaptor binding site was deleted (TBK1ΔC' terminus) (**Figure 3F**). Additionally, we corroborated the immunoprecipitation data with the subcellular location of NAP1 and p-TBK1 during mitosis via immunostaining. Due to the unavailability of antibodies suitable to detect endogenous NAP1 via immunofluorescence, we transiently expressed N'EGFP NAP1 in HeLa cells. NAP1 colocalized with p-TBK1 on the centrosomes of mitotic cells (**Figure 3G- H**). These data suggest that interaction between NAP1 and TBK1

during mitosis is dependent on the C-terminus of both proteins as previously reported for TBK1-adaptor complexes required for innate immune signaling (Ryzhakov and Randow, 2007).

NAP1 is a cell cycle-regulated protein.

We observed a reduction in NAP1 protein in shRNA scramble KD, HeLa, and RPE-1 cell lines when they are synchronized at the G2/M border with nocodazole (**Figure 1F, 4A-B**). This reduction in NAP1 during mitosis also occurred at the mRNA level (**Figure 4C-D**). However, this may not be surprising as global transcription is repressed during mitosis (Prescott and Bender, 1962; Taylor, 1960).

To determine how NAP1 was being temporally regulated on the protein level during mitosis, we examined the stability of NAP1 in both RPE-1 and HeLa lines. Inhibition of protein synthesis with cycloheximide in asynchronous conditions showed that NAP1 was a relatively stable protein (**Figure S4A-B**). Inhibition of lysosomal fusion with chloroquine and thus blocking autophagy also showed no change to NAP1 levels in asynchronous conditions (**Figure S4C-D**). The lower molecular weight lipidated LC3B band increased in chloroquine treated conditions, which is a marker for autophagosomes (**Figure S4C-D, band II**). These data concluded that NAP1 is a relatively stable protein under asynchronous conditions.

To better define when and how NAP1 was decreasing during mitosis, we synchronized cells using the CDK1 inhibitor RO-3306 at G2 and released cells into mitosis. NAP1 was significantly reduced during mitosis 10 minutes after release in both HeLa and RPE-1 cells lines but levels recovered during cytokinesis 60 minutes after release (**Figure 4E-F, lanes 1-3**). NAP1 levels did not degrade 10 minutes after release from G2 with the addition of the proteasome inhibitor MG132. This indicates that the ubiquitin proteasome system (UPS) was involved in this reduction of NAP1 protein level during mitosis (**Figure 4E-F, lanes 2, 4)**. To better characterize

the exact time points that NAP1 levels degrade during mitosis and return to levels seen during asynchronous-G1 conditions, we used the non-transformed RPE-1 cell line. Using p-PLK1 T210 and p-CDK1 Y15 as markers to indicate different stages during mitosis, we saw that NAP1 levels continuously degrade up until 40 minutes (anaphase) after G2 release (**Figure 4G, lane 8,**). Levels began to increase and recover at the 50 and 60 (cytokinesis), and 90-minute time points (asynchronous, G1) (**Figure 4G, lanes 9-11**). We treated another set of cells with the E3 activating enzyme inhibitor TAK243 as an alternative method to inhibit the UPS (Hyer et al., 2018) and saw that NAP1 levels were stabilized throughout the time points collected after G2 release (**Figure 4G**). These data indicate that levels of NAP1 are tightly regulated during mitosis by the UPS.

Mitosis does not elicit an innate immune response.

Previous studies of NAP1 have been limited to understanding its role during innate immunity; therefore, we sought to determine whether this binding of NAP1 during cell cycle progression to TBK1 for its activation at centrosomes activated innate immune pathways. NAP1 is also an adaptor for TBK1 during the innate immune response in which TBK1 on the endoplasmic reticulum or cytosol phosphorylates the transcription factors, interferon regulator factor 3 and 7 (IRF3/IRF7), causing their translocation to the nucleus resulting in the stimulation of the Type I interferon response (Fitzgerald *et al.*, 2003; Goncalves *et al.*, 2011; Ryzhakov and Randow, 2007; Sasai et al., 2005; Sharma et al., 2003). First, we tested whether innate immunity gene expression upregulation occurred during mitosis. Using a human monocytic cell line that is highly responsive to immunogenic stimuli, we first confirmed that this cell line displayed TBK1 activation during mitosis (**Figure 5A**) and after exposure to innate immune responsive stimuli (LPS and poly I:C) (**Figure 5B**). We then assessed expression of a few select cytokines known to

be upregulated (**Figure 5C-D**). During mitosis, cytokine expression was either slightly downregulated or only slightly upregulated (in the case of TNF-α), (**Figure 5E**) indicating that TBK1 activation was not triggering a robust innate immune response during mitosis.

Phosphorylation of either IRF3 or an alternative innate immune kinase (IKKε) that works in conjugation with TBK1 and shares high sequence homology (Tojima *et al.*, 2000), occurred only in response to immunogenic stimuli (LPS and poly I:C) and not during mitosis (**Figure 5F**). Together, these data suggest that although TBK1 activation occurs during mitosis in association with an established innate immune response-associated protein, NAP1, this interaction does not activate innate immunity, and there exists a distinct mitotic NAP1-TBK1 signaling axis at centrosomes.

Discussion

Our study reveals a novel role in mitotic regulation for the known TBK1 adaptor protein, NAP1, which we found to be required for TBK1 activation at the centrosomes during cell division. The interaction between NAP1 and TBK1 at centrosomes during mitosis is independent from its established function during innate immune signaling. Furthermore, we have established that NAP1 is a cell cycle regulatory protein whose levels are controlled by the UPS during mitosis.

Our data supports NAP1 as a required protein for mitosis important for normal cell division – a role distinct from its function in innate immune signaling. Though the NAP1 knockout mouse is viable (Fukasaka et al., 2013), we found that non-transformed cell lines were not amenable to CRISPR- or stable shRNA-mediated knockdown of NAP1 (**data not shown**). The NAP1 KO mouse does display a proliferative defect in GM-dendritic cells (Fukasaka *et al.*, 2013), suggesting that future investigation of this mouse strain may be informative. In contrast, TBK1

KO mice are embryonic lethal at day 14.5 with massive apoptosis of the liver and are rescuable with the loss of TNR receptor signaling (Bonnard et al., 2000). TBK1 loss in a cell-type specific or conditional manner in regions of high cell proliferation could better elucidate how TBK1 balances intracellular kinase signaling in its distinct cellular roles, and in particular, cell cycle regulation. To date, most of the work in the conditional TBK1 mice have examined post-mitotic or fully differentiated cells (Duan et al., 2019; Gerbino et al., 2020; Xiao et al., 2017; Zhu et al., 2019).

Our data asserts that the local subcellular activation of TBK1 not only dictates the turning "on" of distinct cellular process but also the unavailability of TBK1 at other subcellular locales thus maintaining those processes in an "off" state. We and others have described this effect in the cases of both viral infection and mitophagy, in which TBK1 signaling and sequestration at damaged mitochondria impedes cell division as TBK1 is unavailable at centrosomes during the start of mitosis (Onorati *et al.*, 2016; Sarraf *et al.*, 2019). This sequestration of TBK1 may act as a safety measure – allowing cells to carry out necessary repair before committing to cell division. While NAP1 was first identified as an innate immune adaptor (Fujita *et al.*, 2003), TBK1 activation at the centrosomes restricts its ability to activate cytokine expression or IRF transcriptional activation even when bound to NAP1. Other cellular processes that are cell cycle-dependent may also involve this type of localized signaling or sequestration type mechanism. For example, during autophagy, mTOR localization at the lysosome which promotes autophagy is blocked during mitosis due to CDK1 phosphorylation of RAPTOR during mitosis (Odle et al., 2020).

TBK1 is tightly regulated, and our previous data showed abnormal activation and localization upon overexpression of TBK1 (Sarraf *et al.*, 2019). The regulation of NAP1 protein

levels during mitosis may ensure that TBK1 is not abnormally activated or overactivated, nor persists longer than necessary during mitosis. Future studies will have to investigate how NAP1 and TBK1 translocate to centrosomes at the start of mitosis and determine the E3 ligase responsible for the ubiquitination and degradation of NAP1 as cells proceed through mitosis. Tripartite motif 38 (TRIM38) was previously shown to degrade NAP1 in innate immune contexts; however, other reports found TRIM38 targeted other pro-inflammatory proteins such as TNFR-associated factor 6 (TRAF6) and TIR domain-containing adapter TRIF (Xue et al., 2012; Zhao et al., 2012a; Zhao et al., 2012b). To our knowledge, this is the first time it has been shown that NAP1 is regulated by the UPS during mitosis which may be a differential type of TBK1 regulation to decrease TBK1 signaling. TBK1 signaling controlling the Type I interferon response is inactivated by autophagic degradation (Prabakaran et al., 2018).

We further characterized the role of NAP1 and TBK1 during mitosis; however, other reports indicate that genetic influence and external environmental signaling/stimuli can also influence cell proliferation in a TBK1-dependent manner. TBK1's role in cell proliferation was originally described in KRAS mutant cell lines (Barbie et al., 2009); however, KRAS mutations interacting with TBK1 are not the sole driver of the proliferation defect (Pillai *et al.*, 2015). In other cellular contexts, proliferation stimulated by growth factor signaling may be reliant on SINTBAD adaptor activation of TBK1 rather than NAP1 (Zhu *et al.*, 2019). The subcellular localization of TBK1 and its adaptor in these genetic and environmental contexts as well as TBK1 substrates have yet to be described, making it uncertain if the differences in proliferation in these contexts are due to changes in mitosis and cytokinesis. It is possible that other stages of the cell cycle are perturbed. It is also possible that because growth factor signaling and KRAS mutations converge on ERK kinase signaling pathways (Katz et al., 2007; Pylayeva-Gupta et al., 2011),

transcriptional changes may be at play in these other contexts, similar to what is apparent when TBK1 regulates innate immunity and IRF transcriptional activation.

In summary, our study describes a new required role for NAP1/AZI2 during mitosis. We have provided mechanistic insight into its function during cell division by NAP1's ability to activate TBK1. Because most researchers have evaluated TBK1-dependent processes such as mitophagy and innate immunity in asynchronous cell populations, this avenue of research is largely unexplored. Future work to understand how innate immunity, selective autophagy, and cell division intersect is highly attractive as all three are implicated in human diseases such as cancer.

Materials & Methods

Cell culture

HeLa and HEK293T cells were maintained in DMEM high glucose supplemented with 10% FBS, 2mM L-Glutamine, 10mM HEPES, 0.1 mM non-essential amino acids, and 1mM sodium pyruvate. RPE-1 cells were a gift from Dr. Daniela Cimini's lab which were maintained in DMEM/F-12 medium supplemented with 10% FBS. Penta KO and DKO HeLa cells were a gift from Dr. Richard J. Youle's lab. THP1-Lucia™ ISG cells (Invivogen) were maintained in RPMI-1640 Medium with 10% FBS, 2 mM L-glutamine, 25 mM HEPES, 100 µg/ml Normocin™, and Pen-Strep (100 U/ml-100 µg/ml). Cells were routinely tested for mycoplasma contamination by PCR (Southern Biotech).

Antibodies

The following antibodies were used for this study: TBK1/NAK Rabbit mAb (#3504S; Cell Signaling Technology (CST)), pTBK1 Rabbit mAb (Ser172; #5483S; CST), pTBK1 Rabbit mAb Alexa Fluor 488 Conjugate (Ser172; #14586; CST), NAP1/AZI2 Rabbit PolyAb (#15042-1-AP;

298 Proteintech ™), GAPDH (G9545; Sigma) , Vinculin Rabbit mAb (# 700062; Invitrogen), p-H3
299 Rabbit mAb (S10; #53348S; CST), SINTBAD Rabbit mAb (#8605S; CST), TANK Rabbit Ab
300 (#2141S; CST), FLAG M2 Mouse mAb (#F1804-200UG; Sigma), p62 Mouse Ab (#H00008878-
301 M01; Abnova), NBR1 mAb (#H00004077-M01; Abnova), TAX1BP1 (HPA024432;Sigma),
302 Optineurin Rabbit mAb (#10837-1-AP; Proteintech), NDP52 (60732, CST), α-Tubulin Mouse
303 mAb (#T6074-100UL; Sigma), α-Tubulin Rabbit Ab (#2144S; CST), α-Tubulin Rabbit Ab
304 (ab52866;Abcam), GFP antibody (Cat#11814460001 Roche), IKKε Rabbit Ab (#2905S; CST),
305 pIKKε Rabbit Ab (S162; #8766S, CST), HA.11 mAB (#901513; BioLegend), IRF3 Rabbit Ab
306 (#4302, CST), p-IRF3 (S386, ab76493,;Abcam), Plk1 Rabbit Ab (#4513T, CST), p-Plk1
307 (Thr210, # 5472T CST), CREST (SKU:15234; Antibodies Inc.), CDK1/CDC2 (#77055, CST),
308 pCDK1/CDC2 (Tyr15; #4539, CST), LC3 (NB600-1384, Novus).

309 **Additional chemicals**

310 The following chemicals were used for this study: 10ug/ul cycloheximide (AC357420010,
311 Fisher Scientific), 10μm MG132 (NC9937881, Fisher Scientific), 1 μM TAK243 (30108,
312 Cayman Chemical), 50 μM chloroquine diphosphate (C2301100G, Fisher Scientific), and10μM
313 BI605906 (50-203-0195, Fisher Scientific).

314 **Plasmids and constructs**

315 To generate NAP1 rescue lines, NAP1 cDNA was cloned into pDONR223 and transferred into
316 the pHAGE-N'-FLAG-HA-IRES-puro, pHAGE-N'-EGFP-Gaw-IRES-Blast, or pHAGE-C'-
317 EGFP-Gaw-IRES-Blast vectors using LR recombinase (Invitrogen). The pHAGE-N'-FLAG-
318 HA-TBK1 cloning has been described previously (Sarraf *et al.*, 2019) and deposited to Addgene
319 #131791. The following site directed mutagenesis primers were used to generated mutant
320 constructions: NAP1 Δ200-270: TTC ATC AAG TGC AGT TTT GTA TAT GGA TCC GTT

TGT TTG GCT TTC, GAA AGC CAA ACA AAC GGA TCC ATA TAC AAA ACT GCA CTT GAT GAA; TBK1 Δ C' terminus: GGG GAC AAG TTT GTA CAA AAA AGCAGG CTT CG AGG AGA

TAG AAC CATGAT GCA GAG CAC TTC TAA TCA TCT G,

GGG GAC CAC TTT GTA CAA

GAA AGCTGG GTC CTA CTA TAT CCA TTC TTCTGA CTT ATT. All constructs were confirmed by DNA sequencing and deposited on Addgene.

Retrovirus and lentivirus generation

Dishes were coated with 50μg/mL poly-d-lysine (Sigma); and HEK293T cells were plated at 70-80% confluency before transfection. Lentiviral helpers and constructs were transfected using X-tremeGENE 9™ (Roche) according to the manufacturer's instructions at a 1:3 ratio. 24 hrs after transfection, media was changed. Infectious media containing virus was collected 40 hrs later and filtered with a 0.45μm PES membrane filter (Millipore). Live filtered virus was used to transduce cells with polybrene (10μg/ml, Sigma).

CRISPR Knockout Cell Line Generation

In brief, CRISPR design was aided by publicly available software provided by MIT at www.crispr.mit.edu. CRISPR oligos for NAP1: AAA CCA GCT GGA GGA GTT CTA CTT C, CAC CGA AGT AGA ACT CCT CCA GCT G. Primers were annealed with Phusion DNA polymerase (Thermo Fisher Scientific) using the following conditions: 98^{o}C for 1', 2-3 cycles of (98^{o}C for 10", 53^{o}C for 20", 72^{o}C for 30"), 72^{o}C for 5.' The annealed primers were cloned into the linerarized gRNA vector gRNA, which was a gift from Dr. Feng Zhang (Addgene plasmid #62988) using the Gibson Assembly Cloning Kit (NEB). HeLa cells were cotransfected using XtremeGENE 9™ (Roche) using the above CRISPR plasmid. Cells were selected by puromycin

(1mg/ml) and serially diluted into 96 well plates to select for single colony clones. DNA was extracted from individual clones using the Zymo gDNA Isolation Kit and genotyped/sequenced using the following primers: Exon 4 F GAAGCGAATGACATCTGCA, Exon 4 R CCTCTTCTGCTTCATCACAACCT.

shRNA Cell Line Generation

pLKO.1 puro was a gift from Dr. Bob Weinberg (MIT) (Addgene plasmid # 8453) digested with AgeI and EcoRI for 4 hrs at 37^{o}C. Digested plasmid was excised, and gel purified with GeneJET™ gel extraction kit (Thermo Fisher). Oligos were designed for the following target sequences and annealed (NAP1: CCG GCC ACT GCA TTA CTT GGA TCA ACT CGA GTT GAT CCA AGT AAT GCA GTG GTT TTT G; AAT TCA AAA ACC ACT GCA TTA CTT GGA TCA ACT CGA GTT GAT CCA AGT AAT GCA GTG G, TANK: CCG GCC TCA AAG TCT ACG AGA TCA ACT CGA GTT GAT CTC GTA GAC TTT GAG GTT TTT G; AAT TCA AAA ACC TCA AAG TCT ACG AGA TCA ACT CGA GTT GAT CTC GTA GAC TTT GAG G, SINTBAD: CCG GCC TCT GCC TTT CTG TTC TTA ACT CGA GTT AAG AAC AGA AAG GCA GAG GTT TTT G; AAT TCA AAA ACC TCT GCC TTT CTG TTC TTA ACT CGA GTT AAG AAC AGA AAG GCA GAG G). Annealed oligos were ligated into the digested vector with T4 ligase (NEB); and colonies were screened by sequencing. Scramble shRNA was a gift from Dr. David Sabatini (MIT) (Addgene plasmid # 1864). Cells were selected for using 1mg/mL puromycin.

Cell synchronization

Nocodazole treatment: Cells were incubated with 1ug/ml nocodazole (Sigma) containing medium to synchronize at the G2/M border for 16 hours and collected for further experiments.

366 R0-3306 treatment: To synchronize at G2, cells were reversibly incubated with 9μM RO-3306
367 (TCI) containing medium for 20 hrs and collected at the following time points corresponding to
368 their respective cell cycle stages when released in normal growth medium. 0hr – G2; 1hr – M
369 (metaphase); 7hrs – G1. Mitotic shake was employed to obtain maximum number of mitotic
370 cells.

371 **Western blots**

372 For immunoblotting, cells were lysed using 1X RIPA buffer (Thermo scientific Pierce ™ RIPA
373 Buffer) containing 1X protease/phosphatase inhibitor cocktails (Thermo Scientific Halt™).
374 Protein concentration was quantified using DC™ Protein Assay Kit (Bio-Rad). Human tissue
375 samples were obtained using the INSTA-Blot Human Tissues pre-run western blot (Novus
376 Biologicals). Cell lysates were boiled for 15 mins with 2X LDS buffer containing 50 mM DTT,
377 and 20μg of protein lysates were resolved by 4%-12% Bis-Tris gels and transferred to PVDF
378 membranes. Blots were blocked using 5% non-fat powdered milk in 1X TBST (150mM NaCl,
379 20mM Tris, pH 8.0, 0.1% Tween 20). Primary and secondary antibody incubations were carried
380 out in 2.5% non-fat powdered milk in 1X TBST for overnight at 4°C and 1hr at room
381 temperature, respectively. Blots were exposed using Clarity™ Western ECL Substrates (Bio-
382 Rad), ECL™ Select Western Blotting Detection Reagent (GE Healthcare), or SuperSignal™
383 West Femto Maximum Sensitivity Substrate (Thermo Scientific) and detected by the ChemiDoc
384 Imaging System (BioRad).

385 **Immunocytochemistry**

386 Cells for immuno-fluorescence imaging were plated in 6 well cell culture plates (Corning
387 Incorporated) on glass coverslips. Cells were fixed with 4% PFA for 10 mins and permeabilized
388 with 0.1% Triton-X-100 for 10 mins followed by blocking with 10% BSA 5% NGS for 45 mins

389 at RT. Cells were incubated with primary antibodies (diluted in 5% BSA and 2.5% NGS)
390 overnight at 4ºC followed by washing with 1X PBS and incubated with AlexaFluor (Thermo
391 Fisher) conjugated secondary antibodies in the dark for 1 hour. Following the washing step, the
392 cells were stained with .1µg/mL DAPI for 5 mins (Thermo Fisher) and mounted on the slides
393 using Fluoromount (Southern-Biotech). Imaging was carried out using a Nikon C2 confocal
394 microscope. For mitotic index, and multinucleated cell count, and cytokinetic cell count random
395 fields of view were captured for each genotype to sample approximately 1000 cells for each
396 biological replicate (n=3). Mitotic cells were identified by chromosome condensation,
397 kinetochore staining by CREST and verified by α-tubulin morphology. For mitotic defects
398 analysis random fields of view were captured for each genotype to sample approximately 50
399 mitotic cells per biological replicate, and for cytokinetic defects analysis, random fields of view
400 were captured for each genotype to sample approximately 30 cytokinetic cells per biological
401 replicate.

402 **Cell viability assay for growth curve**

403 Approximately, 200 to 400 cells were plated (4 wells/genotype) in white-coated 96-well plates
404 (Brand Tech Scientific) in growth media. Cell growth curve was obtained by CellTiter-Glo®
405 Luminescent Cell Viability Assay (Promgea) using a luminescence reader every 24 hours. Mean
406 cell number corresponding to the luminescence on each day was normalized to the first day in
407 the graph.

408 **Immunoprecipitation**

409 Cells were lysed with the following lysis buffer: 50 mM Tris/HCl pH 7.5, 150 mM NaCl, 1 mM
410 EGTA, 1 mM EDTA, 0.5(v/v) NP-40, 1 mM sodium orthovanadate, 50 mM NaF, 5 mM sodium
411 pyrophosphate, 0.27 M sucrose, 10 mM Na 2-glycerophosphate, 0.2 mM phenylmethylsulphonyl

fluoride, 1x protease/phosphatase inhibitor cocktail (Pierce), and 50 mM iodoacetamide. Cells were incubated for 20 minutes end over end at 4°C then spun at 16,000 x *g* for 15 minutes at 4°C. Supernatant was measured using the Dc™ protein assay (Bio-Rad). 500µg of protein was incubated on magnetic beads (FLAG M2 beads (Sigma), GFP beads (Chromotek) end over end at 4°C for 2 hrs. 2X LDS with 50mM DTT was used to elute protein off the beads, and pH was restored with NaOH.

Transfection

HEK293T cells were plated on poly-d-lysine coated dishes and reverse transfected with 1:1 jetOPTIMUS transfection reagent (Polyplus). Cells were treated the next day with 100ng/ml nocodazole (Sigma) and collected 16hrs later. HeLa cells were reverse transfected with 1:3 or 1:6 X-tremeGENE 9™ (Roche) transfection reagent according to the manufacturer's instructions.

Real Time PCR

RNA was isolated using Trizol Reagent (Ambion Life Technologies) and converted to cDNA using iScript™ (Bio-Rad) per the manufacturer's directions. SYBR Green Supermix (Bio-Rad), 20 ng of cDNA and 0.4 µM of each primer set was mixed in a 10 µl RT-PCR reaction that was ran on the CFX96 System (Bio-Rad). The primers that were used span exons: Actin F: 5' CCCGCCGCCAGCTCACCAT 3', R: 5' CGATGGAGGGGAAGACGGCCC 3'. TANK F: 5' AGCAAGGAGTCTTGGCAGTC 3', R: 5' GCACTGTGTTTCAGTTGCAGT 3'. SINTBAD F: 5' ACCAGTTCCAGCATGAGTTACA 3', R: 5' TCTCCCTCAGCTCTGTCTCC 3'. AZI2 F: 5' AGGTGGAAACTCAGCAGGTG 3', R: 5' ATGGATCCGTTTGTTTGGCT 3'. IL-6 F: 5' AGCCACTCACCTCCTCAGAACGAA 3', R: 5' AGTGCCTCTTTGCTGCTTTCACAC 3'. TNF-α F: 5' TCAATCGGCCCGACTATCTC 3', R: 5' CAGGGCAATGATCCCAAAGT 3'. IL-

435 10 F: 5' AAGACCCAGACATCAAGGCG 3', R: 5' CAGGGAAGAAATCGATGACAGC 3'.
436 RT-PCR was performed in triplicate wells from three independent biological experiments.
437 Expression levels were normalized to β-actin and fold change was determined by comparative C_T
438 method.

439 **Statistical Analysis**

440 For comparisons between two groups, student's t-test was used to determine statistical
441 significance. Ordinary one-way ANOVA followed by Tukey's multiple comparisons were used
442 for three or more groups using GraphPad Prism software. Differences in means were considered
443 significant if $p < 0.05$ and designated as the following $p<0.05$ - *; $p< 0.01$ - **; $p< 0.001$ - ***.
444 $p<.0001$ - ****; ns – not significant.

445 **Acknowledgments**
446
447 This work was supported in part by the National Institutes of Health Grants GM142368 and
448 departmental startup funds (AMP). We also thank Dr. Daniela Cimini and Mathew Bloomfield
449 for advice, reagents, and their expertise. The authors declare no competing financial interests.

450 **Author Contributions**

451 S.P. planned and performed experiments, analyzed data, wrote the manuscript, and revised the
452 manuscript. S.A.S planned and performed experiments, analyzed data, provided reagents, and
453 revised the manuscript. L.Z., L.E.F, and N.D performed experiments. A.O. planned experiments
454 and analyzed data. A.M.P. conceived project, planned experiments, performed experiments,
455 analyzed data, and wrote and revised the manuscript. All authors read and approved the
456 manuscript.

457 **Figure Legends**

458 **Figure 1: NAP1/AZI2 is required for TBK1 activation during mitosis.**

(**A-C)** qRT-PCR showing relative expression of TANK1 (A), SINTBAD (B) and NAP1 (C) mRNA levels normalized to β-actin stably expressing shRNAs. n=3 independent experiments. Error bars ±SD.

(D-F) Western blot analysis of p-TBK1 in asynchronous and synchronized mitotic cells from scramble control, and cell lines stably expressing TANK (D), SINTBAD (E), and NAP1 (F) shRNAs, respectively. GAPDH was used as a loading control.

Figure 2: NAP1 KO cells have mitotic and cytokinetic defects similar to TBK1 KO cells.

(A) Western blot analysis of p-TBK1 in asynchronous and mitotic cells from HeLa, NAP1 KO clone 10, and NAP1 KO clone 12. GAPDH was used as a loading control.

(B) Relative intensity of pTBK1 on centrosomes of mitotic cells from HeLa and NAP1 KO cells. 40-50 mitotic cells per group were quantified from 2 biological replicates.

(C) Representative confocal images of pTBK1 expression on mitotic centrosomes from HeLa and NAP1 KO cells. DAPI (blue) was used as a nuclear counterstain (on composite image), α-Tubulin for cytoskeleton staining (red), and pTBK1 S172 conjugated 488 (green). Scale bar, 20 μm, insets.

(**D)** Growth curve with normalized luminescence for HeLa cells, NAP1 KO clone 10 and NAP1 KO clone 12**.** Error bars indicate ±SD for technical replicates.

(**E-G)** Mitotic (E), multinucleated (F), and abnormal mitotic (G) cell counts from an asynchronous population of HeLa, TBK1, and NAP1 KO cells. Error bars indicate ±SD; n=3 independent experiments. For mitotic index and multinucleated cell count, random fields of view were captured sampling approximately 1000 cells per biological replicate from each genotype. For abnormal mitotic cell counts, random fields of view were captured to sample approximately 50 mitotic cells per biological replicate from each genotype.

(**H)** Pie chart representing the percentage of different types of mitotic defects found in HeLa, TBK1, and NAP1 KO cells. At least 50 mitotic cells per biological replicate from each genotype were analyzed. n=3 independent experiments. * p <.05, ** p <.01 compared to HeLa.

(**I**) Representative confocal images of NAP1 KO mitotic defects: (i) multipolar metaphase, (ii) multipolar prometaphase, and (iii) monopolar prometaphase/metaphase cells. DAPI (blue) was used as a nuclear counterstain, α-Tubulin for cytoskeleton staining (green), and CREST for kinetochore staining (red). Scale bar, 20 μm, insets, 5μm.

(**H**) Western blot analysis of p-TBK1 in asynchronous and synchronized mitotic cells from HeLa, NAP1 KO clone 12, and the stable NAP1 rescue line. GAPDH was used as a loading control.

Figure 3: NAP1 binds to TBK1 during mitosis and is localized to centrosomes.

(A) Cartoon representing protein domains of full length (FL) TBK1, TBK1 lacking adaptor binding domain (Δ C' terminal), FL NAP1, and NAP1 lacking the TBK1 binding domain (Δ200-270).

(**B)** Representative immunoblots of the pulldown of GFP-NAP1 or GFP-NAP1 Δ200-270 in asynchronous and synchronized mitotic cells.

C) Quantification of the ratio of pTBK1/TBK1 signal after normalization to the pulldown efficiency Error bars indicate ±SD; n = 3 independent experiments.

(**D)** Representative immunoblots of the pulldown of TBK1 in asynchronous and synchronized mitotic cells in TBK1 rescue cell lines.

(E) Quantification of the ratio of NAP1 signal after normalization to the pulldown efficiency of TBK1. Error bars indicate ± SEM; n = 3 independent experiments.

(**F)** Representative immunoblots of the pulldown of TBK1 and TBK1 lacking adaptor binding domain Δ C' terminal in synchronized mitotic cells.

(**G)** Representative confocal images of HeLa cells transiently expressing EGFP-NAP1 with immunocytochemical detection of p-TBK1. White arrow depicts area used for line scan analysis in (H). Scale bar = 20μm, inset = 5μm.

(H) Line scan analysis of images in (G) generated from Nikon Elements software.

Figure 4: NAP1 is a cell cycle regulated protein.

(A-B) Western blot analysis of NAP1 in asynchronous and synchronized mitotic cells from HeLa (A) and RPE-1 (B) cells. GAPDH was used as a loading control.

(**C-D)** NAP1 mRNA expression normalized relative to actin in asynchronous and synchronized mitotic HeLa (C) and RPE-1 (D) cells. Error bars indicate ±SD; n = 3 independent experiments.

(**E-F)** Western blot analysis of NAP1 protein level after MG132 treatment after G2 release in HeLa (E) and RPE-1 (F) cells. Vinculin or GAPDH was used as a loading control.

(G) Western blot analysis of NAP1 after TAK243 treatment after G2 release in RPE-1 cells. Vinculin was used as a loading control.

Figure 5: Mitosis does not elicit an innate immune response.

(A) Western blot analysis of THP-1 cells synchronized at G2, M, or G1-Async to determine p-TBK1 levels. Actin was used as a loading control.

(**B)** Western blot analysis of THP-1 cells stimulated with LPS or poly I:C for 1 hrs and 8 hrs, respectively. Blots were probed for p-TBK1 and NAP1. GAPDH was used as a loading control.

(**C-D)** Relative mRNA expression of cytokines upregulated during innate immunity normalized to β-actin when stimulated with LPS (C) for 1 hrs or poly I:C (D) for 8 hrs. Error bars indicate ±SD; n = 3 independent experiments.

(**E)** Relative mRNA expression of cytokines during cell cycle synchronization normalized to β-actin. Error bars indicate ±SD; n = 3 independent experiments.

(**F)** Western blot analysis of p-IRF3 and p-IKKe of THP-1 cells synchronized at G2, M, or G1-Async or stimulated with LPS or poly I:C for 1 hrs and 8 hrs, respectively. α-Tubulin was used as a loading control.

Supplementary Figures

Figure S1: Autophagy adaptors are not required for TBK1 activation during mitosis.

(A) Western blot analysis of HeLa and NDP52/optineurin DKO cells in asynchronous and mitotic conditions. β-actin was used as a loading control.

(B) Western blot analysis of HeLa & Penta KO HeLa cells lacking NBR1, TAX1BP1, optineurin, NDP52, p62 in asynchronous and mitotic cells. GAPDH was used as a loading control.

Figure S2: Loss of NAP1 and TBK1 cause similar cytokinetic defects.

(A) Cytokinetic cell count from an asynchronous population of WT HeLa, TBK1 KO and NAP1 KO. Error bars indicate ±SD; n=3 independent experiments. Random fields of view were captured sampling approximately 1000 cells per biological replicate from each genotype.

(B) Abnormal cytokinetic cell count from an asynchronous population of WT HeLa, TBK1 KO and NAP1 KO. Error bars indicate ±SD; n=3 independent experiments. Random fields of view were captured sampling approximately 30-40 cytokinetic cells per biological replicate from each genotype.

(C) Representative confocal images of cytokinetic defects seen in TBK1 KO (i-iii) and NAP1 KO (iv-v): (i) multipolar cytokinesis, (ii) unequal cytokinesis, (iii) combination of unequal multipolar cytokinesis, (iv) multipolar cytokinesis, (v) unequal cytokinesis. DAPI (blue) was

used as a nuclear counterstain, α-Tubulin for cytoskeleton staining (green), and CREST for kinetochore staining (red). Scale bar, 20 μm, insets, 5μm.

(**D**) Pie chart representing the percentage of different types of cytokinetic defects found in HeLa, TBK1, and NAP1 KO cells. * $p < .05$ compared to HeLa.

Figure S3: IKKβ is not an upstream activator of TBK1 during mitosis.

(A) Western blot analysis of multiple different human tissue samples probed for NAP1. Vinculin was used as a loading control. * indicates non-specific bands.

(B) Western blot analysis of HeLa cells at G2 and M. Cells were either collected untreated or treated with BI 605906 for 1 hour. GAPDH was used as a loading control.

(C) Western blot analysis of HeLa and TBK1 KO cells in asynchronous and mitotic cells. Vinculin was used as a loading control.

Figure S4: NAP1 is a relatively stable protein.

(**A-B)** Western blot analysis of NAP1 protein levels after cycloheximide treatment up to 6 hours in HeLa (A) and RPE-1 (B) cells. Vinculin was used as a loading control. **(C-D)** Western blot analysis of NAP1 protein levels after 6 hrs of chloroquine treatment in HeLa (C) and RPE-1 (D) cells. Vinculin was used as a loading control.

References

Bakshi, S., Taylor, J., Strickson, S., McCartney, T., and Cohen, P. (2017). Identification of TBK1 complexes required for the phosphorylation of IRF3 and the production of interferon beta. Biochem J *474*, 1163-1174. 10.1042/BCJ20160992.

Barbie, D.A., Tamayo, P., Boehm, J.S., Kim, S.Y., Moody, S.E., Dunn, I.F., Schinzel, A.C., Sandy, P., Meylan, E., Scholl, C., et al. (2009). Systematic RNA interference reveals that oncogenic KRAS-driven cancers require TBK1. Nature *462*, 108-112. 10.1038/nature08460.

Bonnard, M., Mirtsos, C., Suzuki, S., Graham, K., Huang, J., Ng, M., Itie, A., Wakeham, A., Shahinian, A., Henzel, W.J., et al. (2000). Deficiency of T2K leads to apoptotic liver degeneration and impaired NF-kappaB-dependent gene transcription. EMBO J *19*, 4976-4985. 10.1093/emboj/19.18.4976.

577 Clark, K., Plater, L., Peggie, M., and Cohen, P. (2009). Use of the pharmacological inhibitor
578 BX795 to study the regulation and physiological roles of TBK1 and IkappaB kinase epsilon: a
579 distinct upstream kinase mediates Ser-172 phosphorylation and activation. J Biol Chem *284*,
580 14136-14146. 10.1074/jbc.M109.000414.

581 Clark, K., Takeuchi, O., Akira, S., and Cohen, P. (2011). The TRAF-associated protein TANK
582 facilitates cross-talk within the IkappaB kinase family during Toll-like receptor signaling. Proc
583 Natl Acad Sci U S A *108*, 17093-17098. 10.1073/pnas.1114194108.

584 Duan, W., Guo, M., Yi, L., Zhang, J., Bi, Y., Liu, Y., Li, Y., Li, Z., Ma, Y., Zhang, G., et al.
585 (2019). Deletion of Tbk1 disrupts autophagy and reproduces behavioral and locomotor
586 symptoms of FTD-ALS in mice. Aging (Albany NY) *11*, 2457-2476. 10.18632/aging.101936.

587 Fagerberg, L., Hallstrom, B.M., Oksvold, P., Kampf, C., Djureinovic, D., Odeberg, J., Habuka,
588 M., Tahmasebpoor, S., Danielsson, A., Edlund, K., et al. (2014). Analysis of the human tissue-
589 specific expression by genome-wide integration of transcriptomics and antibody-based
590 proteomics. Mol Cell Proteomics *13*, 397-406. 10.1074/mcp.M113.035600.

591 Fitzgerald, K.A., McWhirter, S.M., Faia, K.L., Rowe, D.C., Latz, E., Golenbock, D.T., Coyle,
592 A.J., Liao, S.M., and Maniatis, T. (2003). IKKepsilon and TBK1 are essential components of the
593 IRF3 signaling pathway. Nat Immunol *4*, 491-496. 10.1038/ni921.

594 Fu, T., Liu, J., Wang, Y., Xie, X., Hu, S., and Pan, L. (2018). Mechanistic insights into the
595 interactions of NAP1 with the SKICH domains of NDP52 and TAX1BP1. Proc Natl Acad Sci U
596 S A *115*, E11651-E11660. 10.1073/pnas.1811421115.

597 Fu, T., Zhang, M., Zhou, Z., Wu, P., Peng, C., Wang, Y., Gong, X., Li, Y., Wang, Y., Xu, X., et
598 al. (2021). Structural and biochemical advances on the recruitment of the autophagy-initiating
599 ULK and TBK1 complexes by autophagy receptor NDP52. Sci Adv *7*. 10.1126/sciadv.abi6582.

600 Fujita, F., Taniguchi, Y., Kato, T., Narita, Y., Furuya, A., Ogawa, T., Sakurai, H., Joh, T., Itoh,
601 M., Delhase, M., et al. (2003). Identification of NAP1, a regulatory subunit of IkappaB kinase-
602 related kinases that potentiates NF-kappaB signaling. Mol Cell Biol *23*, 7780-7793.
603 10.1128/MCB.23.21.7780-7793.2003.

604 Fukasaka, M., Ori, D., Kawagoe, T., Uematsu, S., Maruyama, K., Okazaki, T., Kozaki, T.,
605 Imamura, T., Tartey, S., Mino, T., et al. (2013). Critical role of AZI2 in GM-CSF-induced
606 dendritic cell differentiation. J Immunol *190*, 5702-5711. 10.4049/jimmunol.1203155.

607 Gatot, J.S., Gioia, R., Chau, T.L., Patrascu, F., Warnier, M., Close, P., Chapelle, J.P., Muraille,
608 E., Brown, K., Siebenlist, U., et al. (2007). Lipopolysaccharide-mediated interferon regulatory
609 factor activation involves TBK1-IKKepsilon-dependent Lys(63)-linked polyubiquitination and
610 phosphorylation of TANK/I-TRAF. J Biol Chem *282*, 31131-31146. 10.1074/jbc.M701690200.

611 Gerbino, V., Kaunga, E., Ye, J., Canzio, D., O'Keeffe, S., Rudnick, N.D., Guarnieri, P., Lutz,
612 C.M., and Maniatis, T. (2020). The Loss of TBK1 Kinase Activity in Motor Neurons or in All
613 Cell Types Differentially Impacts ALS Disease Progression in SOD1 Mice. Neuron *106*, 789-
614 805 e785. 10.1016/j.neuron.2020.03.005.

615 Gleason, C.E., Ordureau, A., Gourlay, R., Arthur, J.S.C., and Cohen, P. (2011). Polyubiquitin
616 binding to optineurin is required for optimal activation of TANK-binding kinase 1 and
617 production of interferon beta. J Biol Chem *286*, 35663-35674. 10.1074/jbc.M111.267567.

618 Goncalves, A., Burckstummer, T., Dixit, E., Scheicher, R., Gorna, M.W., Karayel, E., Sugar, C.,
619 Stukalov, A., Berg, T., Kralovics, R., et al. (2011). Functional dissection of the TBK1 molecular
620 network. PLoS One *6*, e23971. 10.1371/journal.pone.0023971.

621 Hemmi, H., Takeuchi, O., Sato, S., Yamamoto, M., Kaisho, T., Sanjo, H., Kawai, T., Hoshino,
622 K., Takeda, K., and Akira, S. (2004). The roles of two IkappaB kinase-related kinases in
623 lipopolysaccharide and double stranded RNA signaling and viral infection. J Exp Med *199*,
624 1641-1650. 10.1084/jem.20040520.

625 Heo, J.M., Ordureau, A., Paulo, J.A., Rinehart, J., and Harper, J.W. (2015). The PINK1-
626 PARKIN Mitochondrial Ubiquitylation Pathway Drives a Program of OPTN/NDP52
627 Recruitment and TBK1 Activation to Promote Mitophagy. Mol Cell *60*, 7-20.
628 10.1016/j.molcel.2015.08.016.

629 Hyer, M.L., Milhollen, M.A., Ciavarri, J., Fleming, P., Traore, T., Sappal, D., Huck, J., Shi, J.,
630 Gavin, J., Brownell, J., et al. (2018). A small-molecule inhibitor of the ubiquitin activating
631 enzyme for cancer treatment. Nat Med *24*, 186-193. 10.1038/nm.4474.

632 Iwamura, T., Yoneyama, M., Yamaguchi, K., Suhara, W., Mori, W., Shiota, K., Okabe, Y.,
633 Namiki, H., and Fujita, T. (2001). Induction of IRF-3/-7 kinase and NF-kappaB in response to
634 double-stranded RNA and virus infection: common and unique pathways. Genes Cells *6*, 375-
635 388. 10.1046/j.1365-2443.2001.00426.x.

636 Katz, M., Amit, I., and Yarden, Y. (2007). Regulation of MAPKs by growth factors and receptor
637 tyrosine kinases. Biochim Biophys Acta *1773*, 1161-1176. 10.1016/j.bbamcr.2007.01.002.

638 Kim, J.Y., Welsh, E.A., Oguz, U., Fang, B., Bai, Y., Kinose, F., Bronk, C., Remsing Rix, L.L.,
639 Beg, A.A., Rix, U., et al. (2013). Dissection of TBK1 signaling via phosphoproteomics in lung
640 cancer cells. Proc Natl Acad Sci U S A *110*, 12414-12419. 10.1073/pnas.1220674110.

641 Larabi, A., Devos, J.M., Ng, S.L., Nanao, M.H., Round, A., Maniatis, T., and Panne, D. (2013).
642 Crystal structure and mechanism of activation of TANK-binding kinase 1. Cell Rep *3*, 734-746.
643 10.1016/j.celrep.2013.01.034.

644 Lazarou, M., Sliter, D.A., Kane, L.A., Sarraf, S.A., Wang, C., Burman, J.L., Sideris, D.P., Fogel,
645 A.I., and Youle, R.J. (2015). The ubiquitin kinase PINK1 recruits autophagy receptors to induce
646 mitophagy. Nature *524*, 309-314. 10.1038/nature14893.

647 Li, F., Xie, X., Wang, Y., Liu, J., Cheng, X., Guo, Y., Gong, Y., Hu, S., and Pan, L. (2016).
648 Structural insights into the interaction and disease mechanism of neurodegenerative disease-
649 associated optineurin and TBK1 proteins. Nat Commun *7*, 12708. 10.1038/ncomms12708.

650 Liu, S., Cai, X., Wu, J., Cong, Q., Chen, X., Li, T., Du, F., Ren, J., Wu, Y.T., Grishin, N.V., and
651 Chen, Z.J. (2015). Phosphorylation of innate immune adaptor proteins MAVS, STING, and
652 TRIF induces IRF3 activation. Science *347*, aaa2630. 10.1126/science.aaa2630.

653 Ma, X., Helgason, E., Phung, Q.T., Quan, C.L., Iyer, R.S., Lee, M.W., Bowman, K.K.,
654 Starovasnik, M.A., and Dueber, E.C. (2012). Molecular basis of Tank-binding kinase 1
655 activation by transautophosphorylation. Proc Natl Acad Sci U S A *109*, 9378-9383.
656 10.1073/pnas.1121552109.

657 Maan, M., Agrawal, N.J., Padmanabhan, J., Leitzinger, C.C., Rivera-Rivera, Y., Saavedra, H.I.,
658 and Chellappan, S.P. (2021). Tank Binding Kinase 1 modulates spindle assembly checkpoint
659 components to regulate mitosis in breast and lung cancer cells. Biochim Biophys Acta Mol Cell
660 Res *1868*, 118929. 10.1016/j.bbamcr.2020.118929.

661 Moore, A.S., and Holzbaur, E.L. (2016). Dynamic recruitment and activation of ALS-associated
662 TBK1 with its target optineurin are required for efficient mitophagy. Proc Natl Acad Sci U S A
663 *113*, E3349-3358. 10.1073/pnas.1523810113.

664 Odle, R.I., Walker, S.A., Oxley, D., Kidger, A.M., Balmanno, K., Gilley, R., Okkenhaug, H.,
665 Florey, O., Ktistakis, N.T., and Cook, S.J. (2020). An mTORC1-to-CDK1 Switch Maintains
666 Autophagy Suppression during Mitosis. Mol Cell *77*, 228-240 e227.
667 10.1016/j.molcel.2019.10.016.

668 Onorati, M., Li, Z., Liu, F., Sousa, A.M.M., Nakagawa, N., Li, M., Dell'Anno, M.T., Gulden,
669 F.O., Pochareddy, S., Tebbenkamp, A.T.N., et al. (2016). Zika Virus Disrupts Phospho-TBK1
670 Localization and Mitosis in Human Neuroepithelial Stem Cells and Radial Glia. Cell Rep *16*,
671 2576-2592. 10.1016/j.celrep.2016.08.038.

672 Pillai, S., Nguyen, J., Johnson, J., Haura, E., Coppola, D., and Chellappan, S. (2015). Tank
673 binding kinase 1 is a centrosome-associated kinase necessary for microtubule dynamics and
674 mitosis. Nat Commun *6*, 10072. 10.1038/ncomms10072.

675 Pomerantz, J.L., and Baltimore, D. (1999). NF-kappaB activation by a signaling complex
676 containing TRAF2, TANK and TBK1, a novel IKK-related kinase. EMBO J *18*, 6694-6704.
677 10.1093/emboj/18.23.6694.

678 Pourcelot, M., Zemirli, N., Silva Da Costa, L., Loyant, R., Garcin, D., Vitour, D., Munitic, I.,
679 Vazquez, A., and Arnoult, D. (2016). The Golgi apparatus acts as a platform for TBK1 activation
680 after viral RNA sensing. BMC Biol *14*, 69. 10.1186/s12915-016-0292-z.

681 Prabakaran, T., Bodda, C., Krapp, C., Zhang, B.C., Christensen, M.H., Sun, C., Reinert, L., Cai,
682 Y., Jensen, S.B., Skouboe, M.K., et al. (2018). Attenuation of cGAS-STING signaling is
683 mediated by a p62/SQSTM1-dependent autophagy pathway activated by TBK1. EMBO J *37*.
684 10.15252/embj.201797858.

685 Prescott, D.M., and Bender, M.A. (1962). Synthesis of RNA and protein during mitosis in
686 mammalian tissue culture cells. Exp Cell Res *26*, 260-268. 10.1016/0014-4827(62)90176-3.

687 Pylayeva-Gupta, Y., Grabocka, E., and Bar-Sagi, D. (2011). RAS oncogenes: weaving a
688 tumorigenic web. Nat Rev Cancer *11*, 761-774. 10.1038/nrc3106.

689 Ravenhill, B.J., Boyle, K.B., von Muhlinen, N., Ellison, C.J., Masson, G.R., Otten, E.G.,
690 Foeglein, A., Williams, R., and Randow, F. (2019). The Cargo Receptor NDP52 Initiates
691 Selective Autophagy by Recruiting the ULK Complex to Cytosol-Invading Bacteria. Mol Cell
692 *74*, 320-329 e326. 10.1016/j.molcel.2019.01.041.

693 Richter, B., Sliter, D.A., Herhaus, L., Stolz, A., Wang, C., Beli, P., Zaffagnini, G., Wild, P.,
694 Martens, S., Wagner, S.A., et al. (2016). Phosphorylation of OPTN by TBK1 enhances its
695 binding to Ub chains and promotes selective autophagy of damaged mitochondria. Proc Natl
696 Acad Sci U S A *113*, 4039-4044. 10.1073/pnas.1523926113.

697 Ryzhakov, G., and Randow, F. (2007). SINTBAD, a novel component of innate antiviral
698 immunity, shares a TBK1-binding domain with NAP1 and TANK. EMBO J *26*, 3180-3190.
699 10.1038/sj.emboj.7601743.

700 Sarraf, S.A., Sideris, D.P., Giagtzoglou, N., Ni, L., Kankel, M.W., Sen, A., Bochicchio, L.E.,
701 Huang, C.H., Nussenzweig, S.C., Worley, S.H., et al. (2019). PINK1/Parkin Influences Cell
702 Cycle by Sequestering TBK1 at Damaged Mitochondria, Inhibiting Mitosis. Cell Rep *29*, 225-
703 235 e225. 10.1016/j.celrep.2019.08.085.

704 Sasai, M., Oshiumi, H., Matsumoto, M., Inoue, N., Fujita, F., Nakanishi, M., and Seya, T.
705 (2005). Cutting Edge: NF-kappaB-activating kinase-associated protein 1 participates in
706 TLR3/Toll-IL-1 homology domain-containing adapter molecule-1-mediated IFN regulatory
707 factor 3 activation. J Immunol *174*, 27-30. 10.4049/jimmunol.174.1.27.

708 Sharma, S., tenOever, B.R., Grandvaux, N., Zhou, G.P., Lin, R., and Hiscott, J. (2003).
709 Triggering the interferon antiviral response through an IKK-related pathway. Science *300*, 1148-
710 1151. 10.1126/science.1081315.

711 Tanaka, Y., and Chen, Z.J. (2012). STING specifies IRF3 phosphorylation by TBK1 in the
712 cytosolic DNA signaling pathway. Sci Signal *5*, ra20. 10.1126/scisignal.2002521.

713 Taylor, J.H. (1960). Nucleic acid synthesis in relation to the cell division cycle. Ann N Y Acad
714 Sci *90*, 409-421. 10.1111/j.1749-6632.1960.tb23259.x.

715 Thurston, T.L., Boyle, K.B., Allen, M., Ravenhill, B.J., Karpiyevich, M., Bloor, S., Kaul, A.,
716 Noad, J., Foeglein, A., Matthews, S.A., et al. (2016). Recruitment of TBK1 to cytosol-invading
717 Salmonella induces WIPI2-dependent antibacterial autophagy. EMBO J *35*, 1779-1792.
718 10.15252/embj.201694491.

719 Thurston, T.L., Ryzhakov, G., Bloor, S., von Muhlinen, N., and Randow, F. (2009). The TBK1
720 adaptor and autophagy receptor NDP52 restricts the proliferation of ubiquitin-coated bacteria.
721 Nat Immunol *10*, 1215-1221. 10.1038/ni.1800.

722 Tojima, Y., Fujimoto, A., Delhase, M., Chen, Y., Hatakeyama, S., Nakayama, K., Kaneko, Y.,
723 Nimura, Y., Motoyama, N., Ikeda, K., et al. (2000). NAK is an IkappaB kinase-activating kinase.
724 Nature *404*, 778-782. 10.1038/35008109.

725 Vargas, J.N.S., Wang, C., Bunker, E., Hao, L., Maric, D., Schiavo, G., Randow, F., and Youle,
726 R.J. (2019). Spatiotemporal Control of ULK1 Activation by NDP52 and TBK1 during Selective
727 Autophagy. Mol Cell *74*, 347-362 e346. 10.1016/j.molcel.2019.02.010.

728 Wild, P., Farhan, H., McEwan, D.G., Wagner, S., Rogov, V.V., Brady, N.R., Richter, B., Korac,
729 J., Waidmann, O., Choudhary, C., et al. (2011). Phosphorylation of the autophagy receptor
730 optineurin restricts Salmonella growth. Science *333*, 228-233. 10.1126/science.1205405.

731 Wong, Y.C., and Holzbaur, E.L. (2014). Optineurin is an autophagy receptor for damaged
732 mitochondria in parkin-mediated mitophagy that is disrupted by an ALS-linked mutation. Proc
733 Natl Acad Sci U S A *111*, E4439-4448. 10.1073/pnas.1405752111.

734 Xiao, Y., Zou, Q., Xie, X., Liu, T., Li, H.S., Jie, Z., Jin, J., Hu, H., Manyam, G., Zhang, L., et al.
735 (2017). The kinase TBK1 functions in dendritic cells to regulate T cell homeostasis,
736 autoimmunity, and antitumor immunity. J Exp Med *214*, 1493-1507. 10.1084/jem.20161524.

737 Xue, Q., Zhou, Z., Lei, X., Liu, X., He, B., Wang, J., and Hung, T. (2012). TRIM38 negatively
738 regulates TLR3-mediated IFN-beta signaling by targeting TRIF for degradation. PLoS One *7*,
739 e46825. 10.1371/journal.pone.0046825.

740 Zhang, C., Shang, G., Gui, X., Zhang, X., Bai, X.C., and Chen, Z.J. (2019). Structural basis of
741 STING binding with and phosphorylation by TBK1. Nature *567*, 394-398. 10.1038/s41586-019-
742 1000-2.

743 Zhao, W., Wang, L., Zhang, M., Wang, P., Yuan, C., Qi, J., Meng, H., and Gao, C. (2012a).
744 Tripartite motif-containing protein 38 negatively regulates TLR3/4- and RIG-I-mediated IFN-
745 beta production and antiviral response by targeting NAP1. J Immunol *188*, 5311-5318.
746 10.4049/jimmunol.1103506.

747 Zhao, W., Wang, L., Zhang, M., Yuan, C., and Gao, C. (2012b). E3 ubiquitin ligase tripartite
748 motif 38 negatively regulates TLR-mediated immune responses by proteasomal degradation of
749 TNF receptor-associated factor 6 in macrophages. J Immunol *188*, 2567-2574.
750 10.4049/jimmunol.1103255.

751 Zhu, L., Li, Y., Xie, X., Zhou, X., Gu, M., Jie, Z., Ko, C.J., Gao, T., Hernandez, B.E., Cheng, X.,
752 and Sun, S.C. (2019). TBKBP1 and TBK1 form a growth factor signalling axis mediating
753 immunosuppression and tumourigenesis. Nat Cell Biol *21*, 1604-1614. 10.1038/s41556-019-
754 0429-8.
755

756

Figure 1

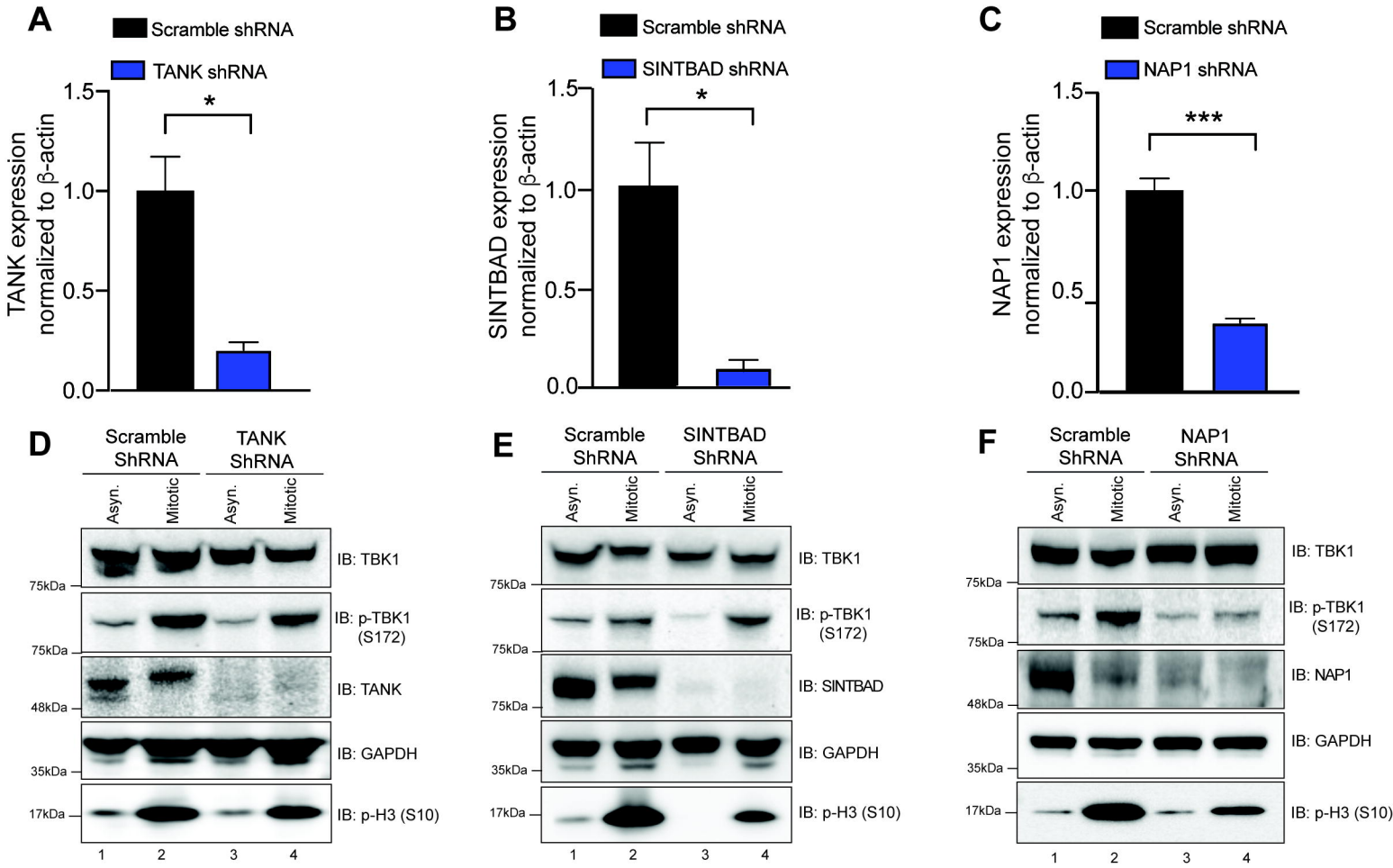
A
Scramble shRNA
TANK shRNA
TANK expression normalized to β-actin
1.5
1.0
0.5
0.0
*
B
Scramble shRNA
SINTBAD shRNA
SINTBAD expression normalized to β-actin
1.5
1.0
0.5
0.0
*
C
Scramble shRNA
NAP1 shRNA
NAP1 expression normalized to β-actin
1.5
1.0
0.5
0.0
***
D
Scramble ShRNA
TANK ShRNA
Asyn.
Mitotic
Asyn.
Mitotic
IB: TBK1
IB: p-TBK1 (S172)
IB: TANK
IB: GAPDH
IB: p-H3 (S10)
75kDa
75kDa
48kDa
35kDa
17kDa
1
2
3
4
E
Scramble ShRNA
SINTBAD ShRNA
Asyn.
Mitotic
Asyn.
Mitotic
IB: TBK1
IB: p-TBK1 (S172)
IB: SINTBAD
IB: GAPDH
IB: p-H3 (S10)
75kDa
75kDa
75kDa
35kDa
17kDa
1
2
3
4
F
Scramble ShRNA
NAP1 ShRNA
Asyn.
Mitotic
Asyn.
Mitotic
IB: TBK1
IB: p-TBK1 (S172)
IB: NAP1
IB: GAPDH
IB: p-H3 (S10)
75kDa
75kDa
48kDa
35kDa
17kDa
1
2
3
4

Figure 2

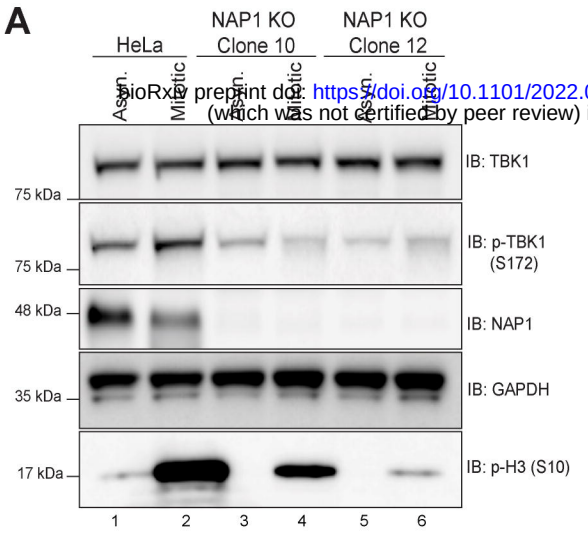

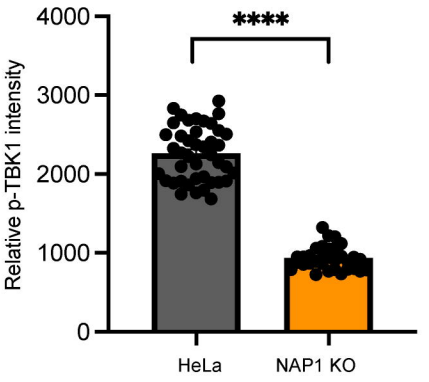

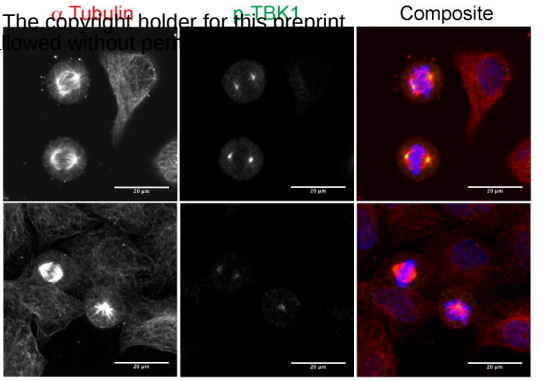

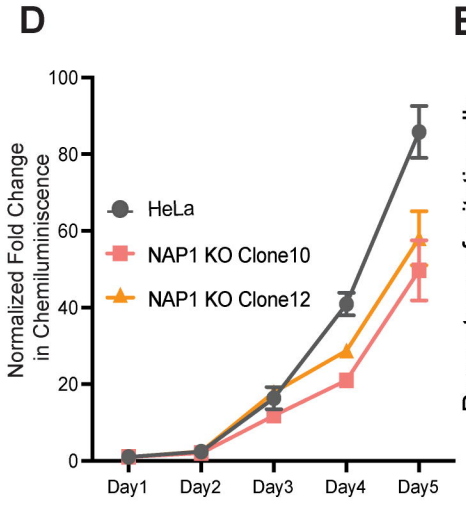

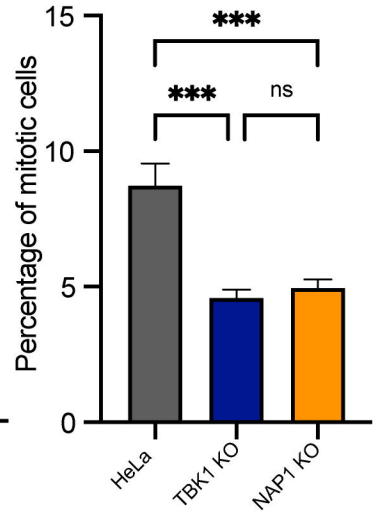

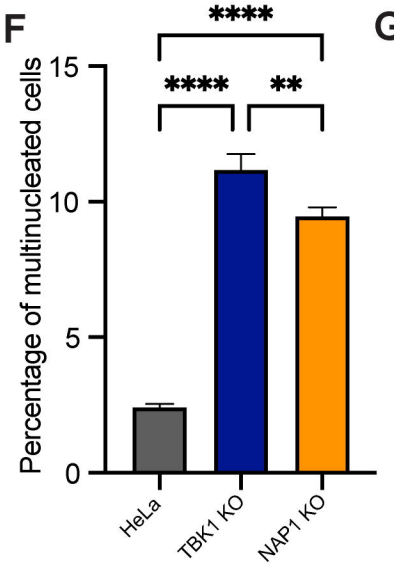

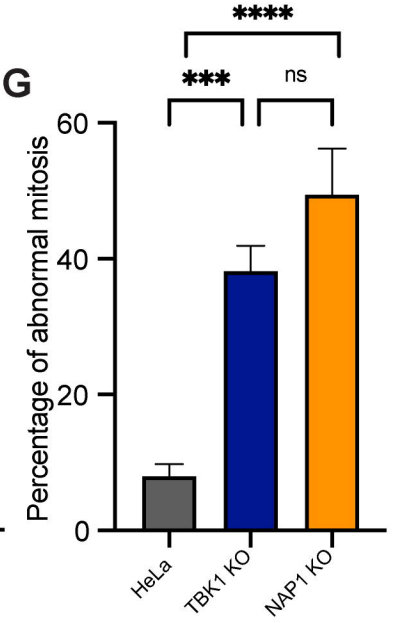

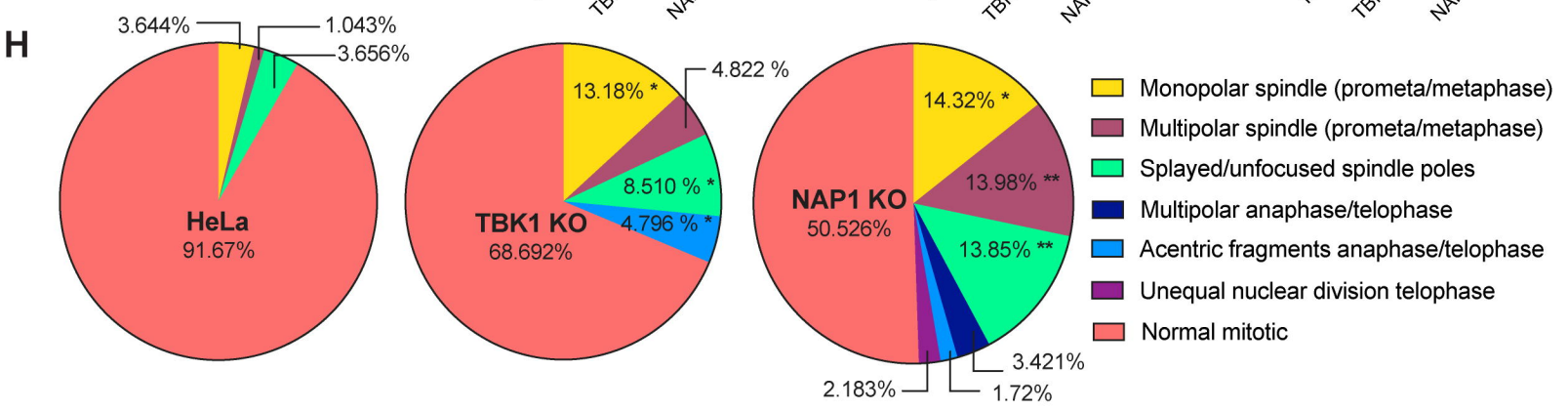

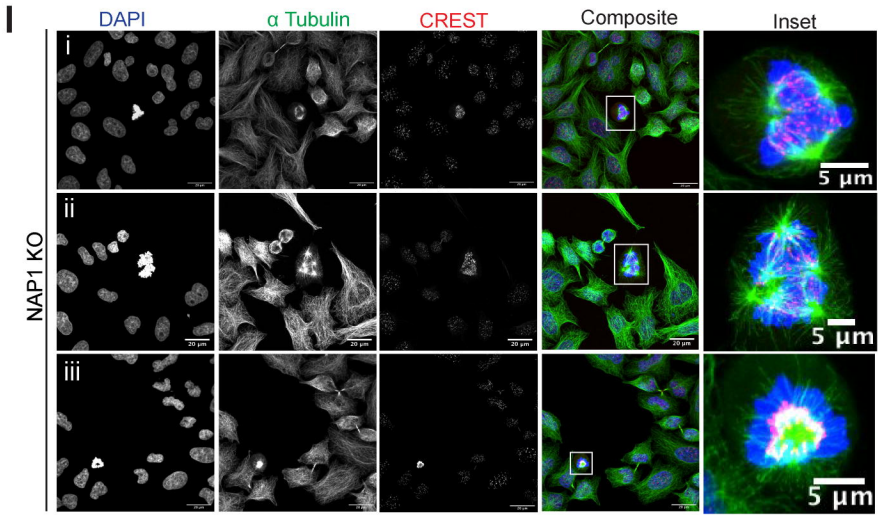

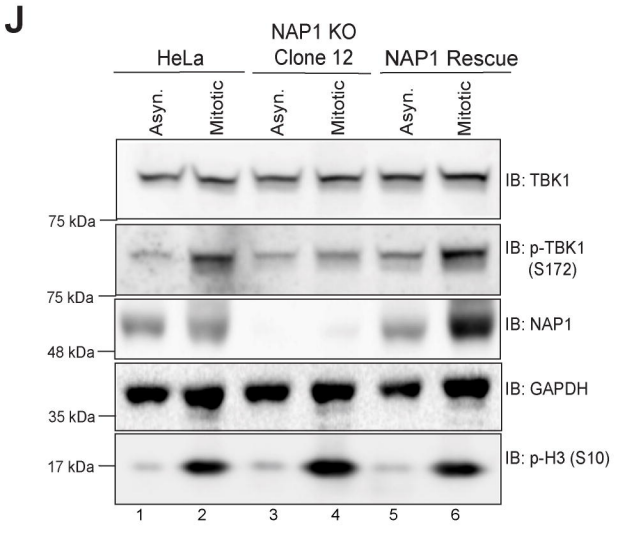

Figure 3

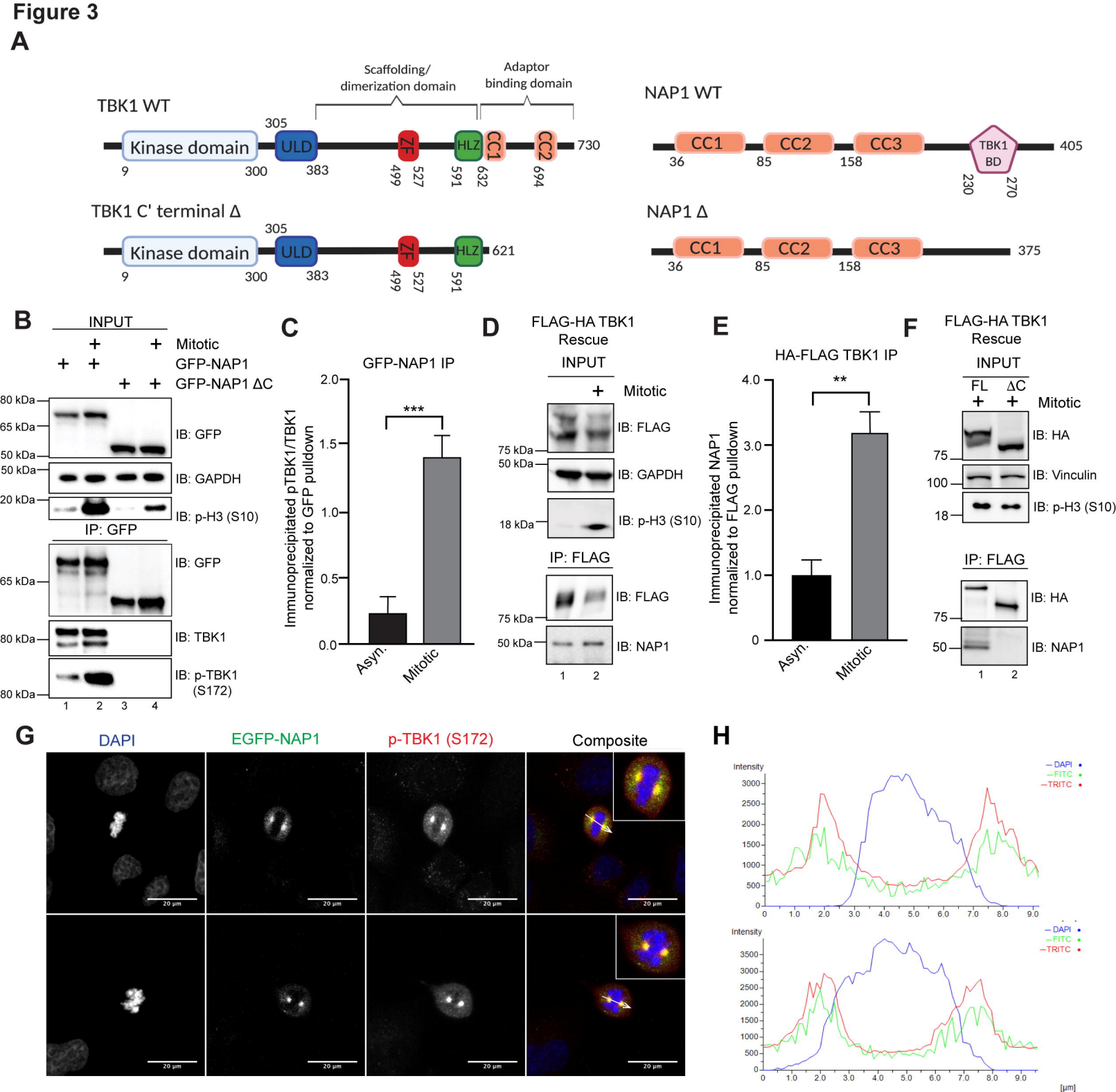
A
TBK1 WT
Scaffolding/ dimerization domain
Adaptor binding domain
Kinase domain
ULD
ZF
HLZ
CC1
CC2
305
730
9
300
383
499
527
591
632
694
TBK1 C' terminal Δ
621
NAP1 WT
CC1
CC2
CC3
TBK1 BD
405
36
85
158
230
270
NAP1 Δ
375
B
INPUT
Mitotic
GFP-NAP1
GFP-NAP1 ΔC
IB: GFP
IB: GAPDH
IB: p-H3 (S10)
IP: GFP
IB: TBK1
IB: p-TBK1 (S172)
C
GFP-NAP1 IP
Immunoprecipitated pTBK1/TBK1 normalized to GFP pulldown
***
Asyn.
Mitotic
D
FLAG-HA TBK1 Rescue
IB: FLAG
IP: FLAG
IB: NAP1
E
HA-FLAG TBK1 IP
Immunoprecipitated NAP1 normalized to FLAG pulldown
**
F
FL
ΔC
IB: HA
IB: Vinculin
G
DAPI
EGFP-NAP1
p-TBK1 (S172)
Composite
20 μm
H
Intensity
DAPI
FITC
TRITC
[μm]

Figure 4

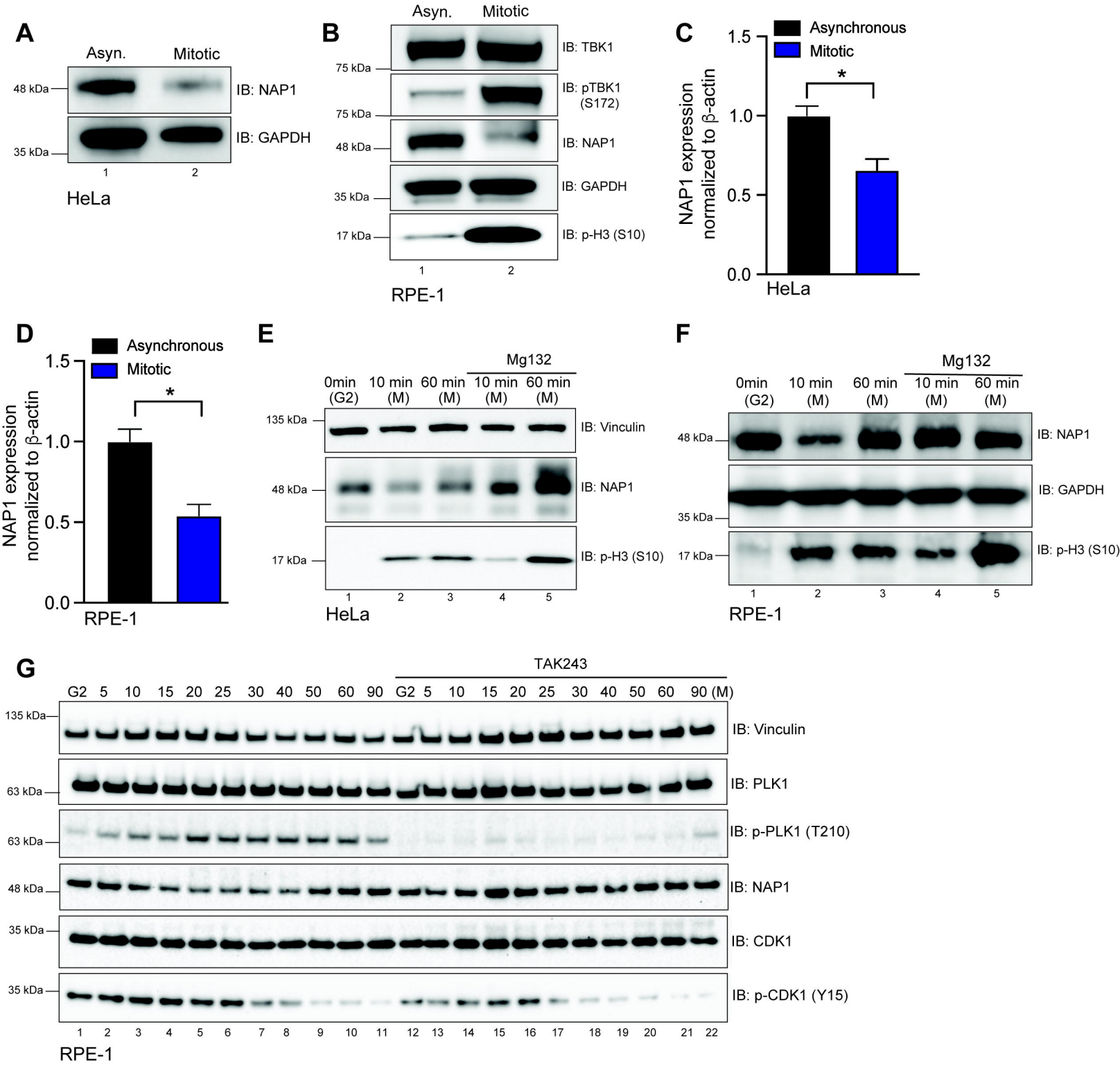
A
Asyn.
Mitotic
48 kDa
IB: NAP1
35 kDa
IB: GAPDH
1
2
HeLa
B
Asyn.
Mitotic
75 kDa
IB: TBK1
75 kDa
IB: pTBK1 (S172)
48 kDa
IB: NAP1
35 kDa
IB: GAPDH
17 kDa
IB: p-H3 (S10)
1
2
RPE-1
C
Asynchronous
Mitotic
*
NAP1 expression normalized to β-actin
1.5
1.0
0.5
0.0
HeLa
D
Asynchronous
Mitotic
*
NAP1 expression normalized to β-actin
1.5
1.0
0.5
0.0
RPE-1
E
Mg132
0min (G2)
10 min (M)
60 min (M)
10 min (M)
60 min (M)
135 kDa
IB: Vinculin
48 kDa
IB: NAP1
17 kDa
IB: p-H3 (S10)
1
2
3
4
5
HeLa
F
Mg132
0min (G2)
10 min (M)
60 min (M)
10 min (M)
60 min (M)
48 kDa
IB: NAP1
IB: GAPDH
35 kDa
17 kDa
IB: p-H3 (S10)
1
2
3
4
5
RPE-1
G
TAK243
G2 5 10 15 20 25 30 40 50 60 90 G2 5 10 15 20 25 30 40 50 60 90 (M)
135 kDa
IB: Vinculin
63 kDa
IB: PLK1
63 kDa
IB: p-PLK1 (T210)
48 kDa
IB: NAP1
35 kDa
IB: CDK1
35 kDa
IB: p-CDK1 (Y15)
1 2 3 4 5 6 7 8 9 10 11 12 13 14 15 16 17 18 19 20 21 22
RPE-1

Figure 5

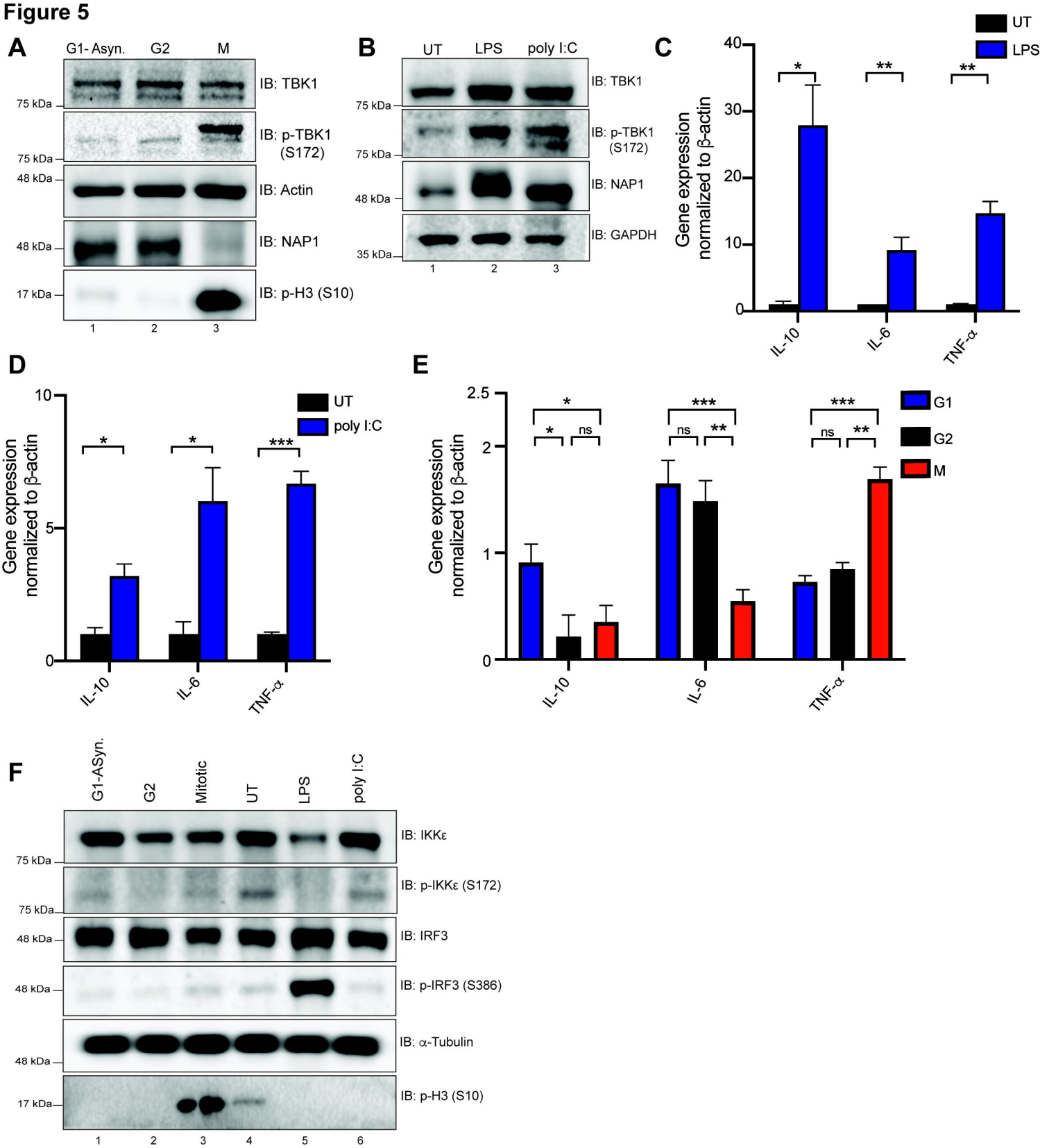
A
G1- Asyn.
G2
M
IB: TBK1
IB: p-TBK1 (S172)
IB: Actin
IB: NAP1
IB: p-H3 (S10)
75 kDa
75 kDa
48 kDa
48 kDa
17 kDa
1
2
3
B
UT
LPS
poly I:C
IB: TBK1
IB: p-TBK1 (S172)
IB: NAP1
IB: GAPDH
75 kDa
75 kDa
48 kDa
35 kDa
1
2
3
C
UT
LPS
Gene expression normalized to β-actin
40
30
20
10
0
*
**
**
IL-10
IL-6
TNF-α
D
UT
poly I:C
Gene expression normalized to β-actin
10
5
0
*
*
***
IL-10
IL-6
TNF-α
E
G1
G2
M
Gene expression normalized to β-actin
2.5
2
1
0
*
*
ns
***
ns
**
***
ns
**
IL-10
IL-6
TNF-α
F
G1-ASyn.
G2
Mitotic
UT
LPS
poly I:C
IB: IKKε
IB: p-IKKε (S172)
IB: IRF3
IB: p-IRF3 (S386)
IB: α-Tubulin
IB: p-H3 (S10)
75 kDa
75 kDa
48 kDa
48 kDa
48 kDa
17 kDa
1
2
3
4
5
6